Eng. Sci., 2022, **18**, 234–242

Engineered Science

DOI: https://dx.doi.org/10.30919/es8d644

A Numerical Study on the Performance of Different Shaped Perforation Hole on the Absorber Duct Insert in a Solar Air Heater

Arunkumar H. S., Shiva Kumar and K. Vasudeva Karanth*

Abstract

The solar air heater (SAH) is one of the solar energy applications used to heat atmospheric air for space heating and drying applications. The convective heat transfer coefficient of the absorber plate is low due to the formation of the laminar viscous sublayer. An attempt is made to improve the efficiency by creating perforation holes of different shapes (circular, triangular and rectangular) on the top surface of the absorber duct insert placed inside the test section of the solar air heater. The absorber duct insert enhances the heat transfer rate, and perforation causes the cross flow and the flow disturbance in the flow stream. A rectangular-shaped hole configuration shows the highest thermal efficiency of 87.01 %, followed by circular and triangular hole configurations. Circular hole configuration shows the highest thermo-hydraulic efficiency of 83.01% at the Reynolds number of 15000.

Keywords: Solar air heater; Perforated duct inserts; Thermo-hydraulic efficiency; Double pass single flow; Crossflow effect.
Received: 10 November 2021; Revised: 02 February 2022; Accepted: 05 February 2022.
Article type: Research article.

1. Introduction

As a renewable energy source, solar energy is widely used for space heating and other applications.[1,2] Solar air heater (SAH) is a passive device that uses solar energy for space heating and drying purposes in commercial and industrial applications. The convective heat transfer coefficient (h) from the absorber plate & air contact to that in the passage is low and causes poor efficiency of the air heater. It is simple in structure, low in maintenance, reliable, and not affected by corrosion or freezing problems.

Researchers experimented with many design variants over the conventional SAH to improve the heat transfer from the absorber surface to the air flowing over it. Various modifications of design studied include the modification of the flow channel, incorporation of turbulators in the flow path, types and number of glazing covers, *etc*.[3,4]

Elfadl *et al*.[5] conducted the experimental study on a double-pass solar air heater in which the mass flow rate was varied for the upper and lower chambers of the absorber plate with the ratio of 1:0, 2:3, 1:3, and 0:1. The authors observed the highest thermal efficiency of 65.21% for the Pin-finned 2:3 mass flow ratio configuration. For the experiments conducted by Yeh *et al*.,[6] on a SAH, a better efficiency was noted for the mass flow ratio 0.5, *i.e.*, when the same quantity of air was distributed above and beneath the absorber plate.

Subramaniam's[7] study on double-pass SAH showed that a lesser gap between the glass cover in a double-pass type gave 10-15% greater efficiency compared to the single-pass solar collector. In a theoretical study conducted by Choudary *et al*.,[8] on the jet impingement SAH, parameters such as hole diameter, plate interspacing, nozzle height, and diameter were varied. The highest rise in temperature and efficiency was 15.5 °C and 26.5%, respectively. Forson *et al*.[9] developed a mathematical model in which air was passed through a two-channel and exited at a single outlet duct. Authors observed the increase in efficiency with the increase in the top to bottom channel ratio for a given overall depth with a simultaneous increase in relative humidity. The authors stated that mass flow rate played a major factor in determining the collector efficiency and a significant increase in the humidity was unfavorable for drying applications. Therefore, the lowest possible duct height is preferable to achieve a higher temperature, but it causes more pressure drop. Hence trade-off is essential while

Department of Mechanical & Manufacturing Engineering, Manipal Institute of Technology, Manipal Academy of Higher Education, Manipal, 576104 India.
**E-mail:* kv.karanth@manipal.edu (K. V. Karanth)

deciding the height of the duct depending on the application of the SAH. Chauhan *et al*.[10] optimized the jet impingent SAH using Taguchi-based design of experimental approach. Sixteen experiments were performed with three main parameters such as jet diameter, and hole pitch in the streamwise and spanwise directions. The authors stated that thermal performance strongly depended on the diameter of the jet (48.8%), followed by spanwise pitch (41%) and streamwise pitch (9.53%). Alsanossi *et al*.[11] performed experiments on jet impingement in a corrugated plate SAH. Results were compared with the conventional duct, flat plate impingement jet, and corrugate plate impingement jet SAH model. The flow rate of air strongly influences the jet impingement effect and hence heat transfer phenomena. The study reveals that corrugated plate impingement helps to break the laminar sub-layer effectively, and thus performance is better than the flat plate and convention model. The authors stated that thermal efficiency increased by 14% with a 3 °C increase in air temperature for an impingent corrugate model. Yadav *et al*.[12] conducted the numerical study using the RNG $k–\varepsilon$ turbulence model and upwind solution scheme. Jet height and diameter were varied for the Reynolds number ranging from 3500 to 17,500. The authors observed that the Nusselt number increased as the Reynolds number increased and a higher value for the lowest diameter was considered. The maximum heat transfer improvement of 7.58 was obtained with the friction factor penalty of 9.1 times for the highest Reynolds number of 17500. The optimum jet diameter ratio of 0.0650 and jet height ratio of 0.216 gave the thermo-hydraulic enhancement factor of 3.66. The performance of a perforated backplate in combination with the absorber plate was studied by Wang *et al*.[13] The mass flow rate ranged from 0.054 to 0.058 kg/s. The study reveals that the flowing air jetting through the back perforation before approaching the duct improved the heat transfer performance. The highest thermal efficiency of 75 % and inlet to the outlet temperature difference of 41 °C were obtained for the flow rate of 0.057 kg/s. Matheswaran *et al*.[14] established the model for the parallel flow jet plate SAH with artificial roughness. In their study, single-pass double duct and single-pass single duct with artificial roughness were incorporated. Out of the various configurations, arc-shaped turbulators presented better performance. The highest energy efficiency ratio of 2.15 and exergy efficiency ratio of 3.4 was observed. Satyender *et al*.[15] carried out the study on the impingement of air jets on the absorber plate of the SAH incorporated with the wavy porous media below the absorber plate. A wavy corrugated plate consisted of 7.66 mm diameter circular holes at the crest region. Better performance was obtained for plate perforation by 48%. Maximum values of thermal efficiency and thermo-hydraulic efficiency of 94% of 84% were noticed. The authors also carried out the perforation impingement jet study on SAH for the configuration with double-pass[16] and attained 18% higher efficiency as compared to the single-pass mode. Serpentine structure with 85% porosity gave a better thermal performance in terms of Nusselt number for the range of mass flow rate tested.

From the comprehensive literature review, it is noted that the effect of different shapes of perforation holes is not explored in a SAH with double pass single flow mode. The nature of pressure and velocity fluctuation varies for different shaped hole shapes. Therefore, it is interesting to focus the research on flow physics in a different shaped hole size in absorber duct insert. The objective of this work is to explore the effect of the triangular, rectangular, and circular-shaped holes on an absorber duct insert in SAH.

2. Methodology

2.1 Experimental section

The pictorial view of the experimental setup is shown in Fig. 1a, and a schematic diagram of the same is provided in Fig. 1b. The test rig is made according to the specifications provided in section 2.2. The experimental test rig is fabricated using plywood, and polystyrene foam insulation is provided on the outside of the duct. The absorber duct with perforations is placed inside the test section and is coated with the black mat finish paint. The inside surface of the duct is provided with glossy laminates to reduce flow losses due to skin friction. The outlet of the collector is connected to the blower via a vortex flow meter and gate valve.

The experiments are conducted at the laboratory ambient conditions for the six values of the mass flow rates ranging from 0.006428 kg/s to 0.038633 kg/s corresponding to the Reynolds number at the inlet, ranging from 3000 to 18000. Solar radiation is simulated using solar simulators which are regulated by the dimmer stat to get the required heat flux. To assume suitable solar insolation for both experimental and numerical studies, a beam radiation value of 950 W/m^2 is set and is determined using a pyranometer at the place of experimentation at 1 PM on a full sunshine day under fair weather conditions during the month of May.

The digital manometer measures the pressure required to pass the air through the duct, and thermocouples are attached to the top of the absorber duct to measure the average temperature at the top surface. Outlet and inlet temperatures are measured by RTD sensors. Forced circulation of the air is created by the air blower, and the mass flow rate is measured with the help of a vortex flow meter.

2.2 Geometric configuration

The geometric model of the SAH is modeled in the ANSYS WORKBENCH tool as shown in Figs. 2a and 2b. It consists of an inlet section, an exit section, and a test section. Dimensions of the sections are taken per ASHRAE standard 93-97[17] and shown in Fig. 2a. Inside the test section, circular, rectangular, and triangular-shaped perforated ducts are separately inserted and analyzed.

2. 3 Mesh generation and grid-independence test

Control volume mesh is generated using the ANSYS workbench tool. Boundary layer mesh is provided near the

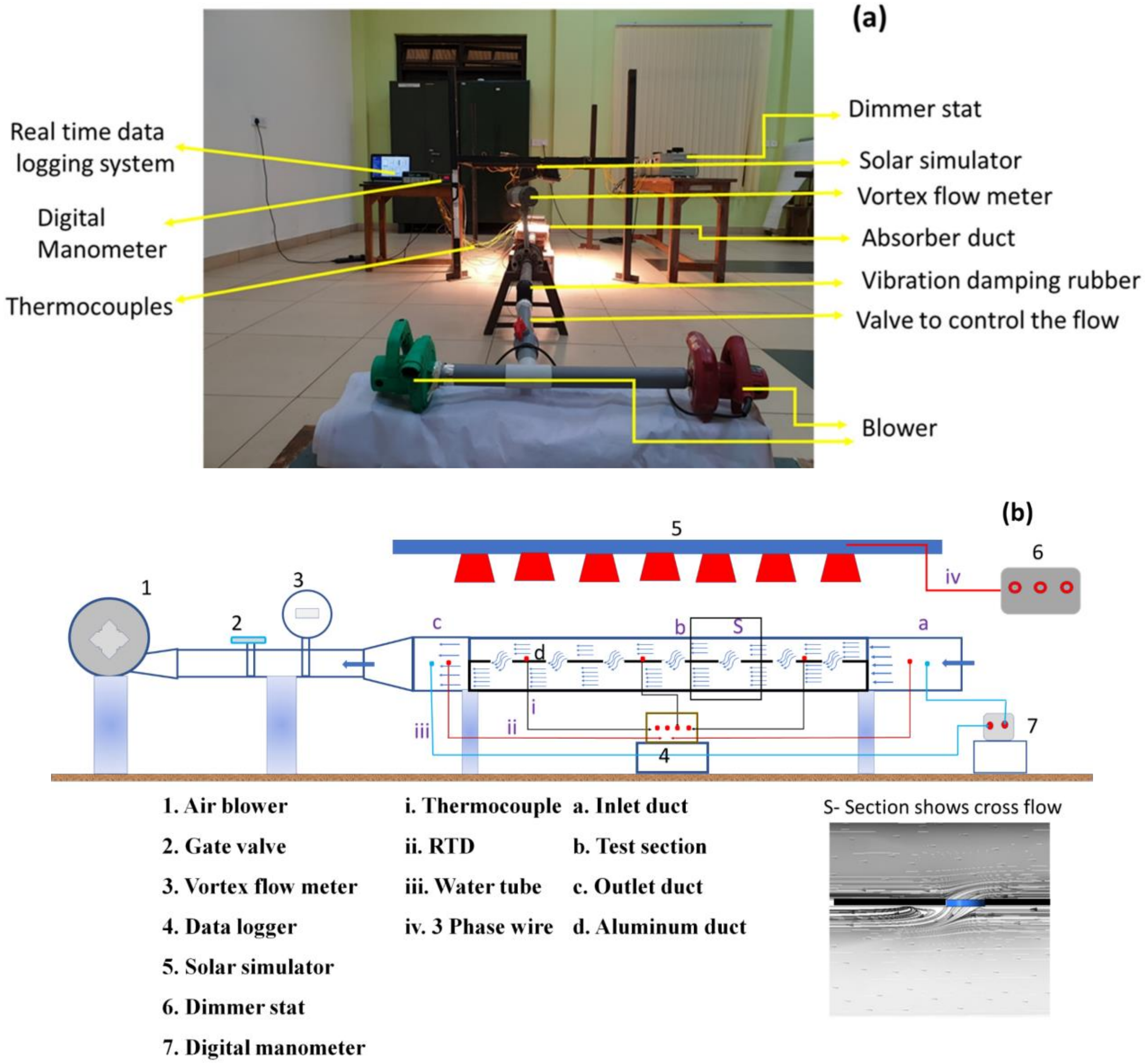

Fig. 1 Solar air heater experimental arrangement (a) Experimental setup (b) Schematic diagram.

interface region of the absorber duct and fluid to capture the boundary layer effects. The non-dimensionalized first layer thickness is approximately unity, *i.e.*, $y+ \approx 1$. The absorber duct with perforation holes is discretized using hexahedral mesh, and the fluid domain meshes with tetrahedron elements. The absorber plate meshed domain with the vents on the top of the absorber duct is shown in Fig. 3.

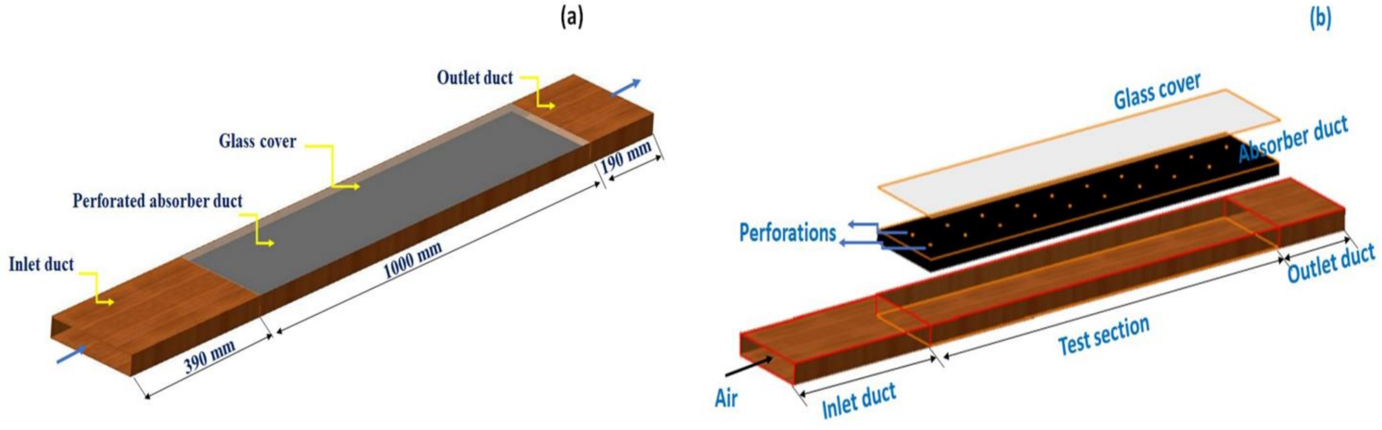

Fig. 2 Geometric model of the Solar air heater (a) Duct inserted SAH (b) Exploded view of the SAH.

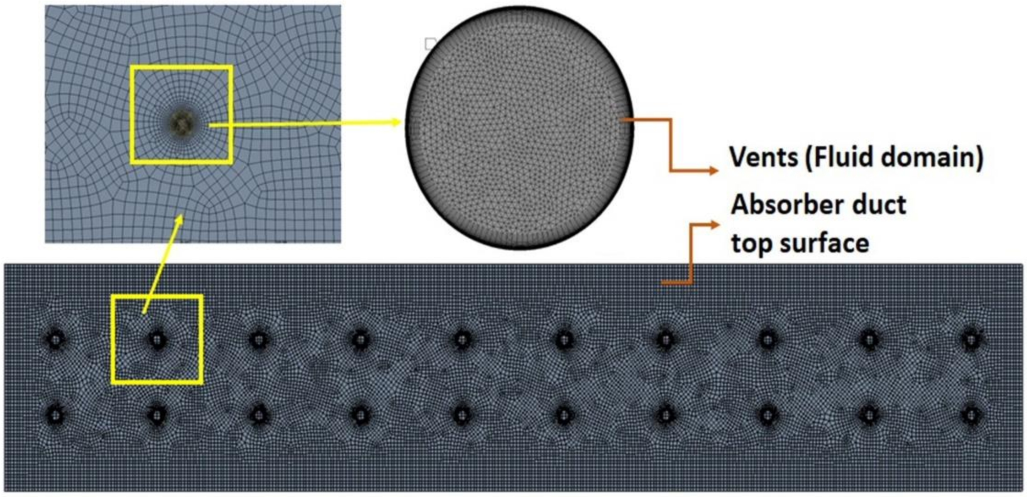

Fig. 3 Mesh generation near the absorber plate vent.

The number of control volume elements adopted in the mesh domain for the plain model varies from 0.6 million to 1.8 million, and the Perforated model varies from 3.6 million to 5.0 million. A grid-independent test is carried out, and the nature of the graph is shown in Fig. 4, where the absorber plate temperature coefficient is plotted against the number of elements. The variation graph is reasonably flat for 1.8 million to 2 million control volumes in the case of the plain model and 4.4 million to 4.6 million for the perforated model. Hence 1.8 million elements for the plain model and 4.4 million control volumes for the perforated model are chosen for further analysis.

2.4 Boundary conditions

The mass flow rate is specified as per the Reynolds number ranging from 3000 to 18000. Inlet is given as a mass flow inlet. The outlet is given as an outflow assuming a fully developed flow condition. Walls are considered as a no-slip boundary condition. The cell zone condition for the absorber duct is taken as aluminum, and the cell zone condition for the fluid part of the domain is taken as air. The material property considered for the analysis is depicted in Table 1. The thermophysical properties of air density, viscosity, and thermal conductivity are invoked as per Eq. (1), Eq. (2), and Eq. (3), respectively. Equations are applicable within the temperature range from 280 K to 470 K.[18]

Table 1. Properties of the material.

Properties	Air	Aluminum	Glass
Specific heat (J/kg K)	1006.3	871	800
Thermal conductivity (W/mK)	Eq. (2)	202.4	1.2
Viscosity (kg/ms)	Eq. (1)	-	-
Density (kg/m^3)	Eq. (3)	2719	2500
Emissivity		0.9	0.925
Refractive index		1	1.53
Specific gas constant (J/kg.K)	287	-	-

$$\rho = 3.9147 - 0.01632 \times T + 2.9013 \times 10^{-5} T^2 - 1.9407 \times 10^{-8} T^3 \quad (1)$$

$$\rho = 3.9147 - 0.01632 \times T + 2.9013 \times 10^{-5} T^2 - 1.9407 \times 10^{-8} T^3 \quad (2)$$

$$k = (0.0015215 + .097459 \times T - 3.3322 \times 10^{-5} T^2) \times 10^{-3} \quad (3)$$

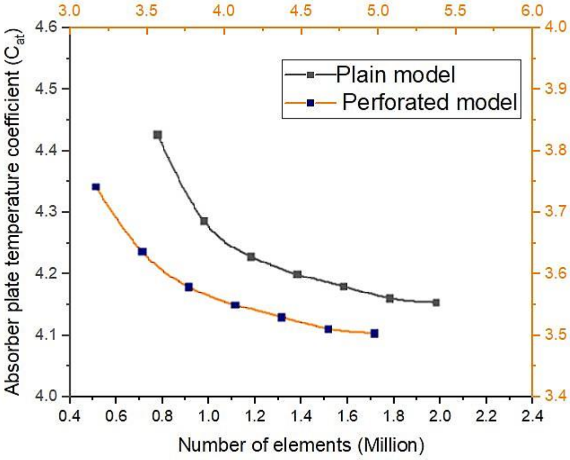

Fig. 4 Grid independent test for the plain model and perforated model at Re = 12000.

The absorber duct top glass surface is invoked with the Discrete Ordinate (DO) radiation model. A longitude of 74.786ºE, a latitude of 13.343ºN, and a GMT of +5.5 is used in the solar load model to define the global position of local solar irradiation condition. This corresponds to 1.00 PM assuming fair weather conditions for the 1st of May and relates to the experimental conditions of the study. A double-precision pressure-based CFD solver is used for numerical simulation. The convergence of the solution is considered when the residuals in the computation domain fall below 10^{-6}.

2.5 Performance parameter

By knowing the air temperature difference between the inlet & outlet of the duct, and solar insolation, thermal efficiency is calculated using Eq. (4). Thermohydraulic efficiency takes into consideration the pumping power required for the fluid flow, hence pressure drop is used to calculate the thermohydraulic efficiency, *i.e.*, given by Eq. (5). Using Eq. (6) nondimensionalized temperature of the absorber plate is calculated.[19]

Thermal efficiency,

$$\eta_{thermal} = \frac{\dot{m}C_p(T_0-T_i)}{I_T A_p} \quad (4)$$

Thermo − hydraulic efficiency,

$$\eta_{thermo-hydraulic} = \frac{\dot{m}C_p(T_0-T_i)-\frac{P_m}{C}}{I_T A_p} \quad (5)$$

Absorber plate temperature coefficient,

$$(C_{at}) = \frac{T_a-T_i}{T_i}X100 \quad (6)$$

Outlet temperature coefficient,

$$(C_{ot}) = \frac{T_o-T_i}{T_i}X100 \quad (7)$$

Where, $\dot{m}$ - Mass flow rate (kg/s); Cp - Specific heat capacity (kJ/kg. K);
I_T - Total radiation input (W); Ap - Area of the absorber plate (m^2); Pm - Pumping power (W);
To – Outlet temperature (K); T_i – Inlet temperature (K); Ta – Absorber plate temperature (K).
Where 'C' is a factor taking into consideration of the overall energy conversion efficiency from thermal to mechanical energy to drive the air blower, and the value is assumed to be 0.18.[20]

2.6 Jet impingement phenomena

Jet impingement is a cross-flow phenomenon whereas this study also involves cross-flow effects induced due to the alteration of the geometry. Jet impingement is induced by forcing the flow through the jet, whereas in this study the crossflow effects are naturally generated due to the pressure difference between the upper and lower chambers along the flow direction. In the present analysis, different geometries of perforations have been made in the absorber plate. When the air flows across them due to the crossflow effects, more turbulence will be induced. This helps to increase the heat transfer rate and thermal efficiency. This study focuses on the influence of different geometrically shaped perforations on thermal performance, which generate the cross-flow effect of different intensities.

2.7 Validation of the numerical result.

Numerical results are validated with the experimental results for the best performing two-row hole diameter of 5 mm, 20 mm duct height configuration.[21] Results are validated in terms of the outlet temperature coefficient calculated using Eq. (7), as shown in Fig. 5. As observed in Fig. 5, numerical and experimental results have matching trend lines, but the numerical values are higher than the experimental results. This is because of the reason to save computational time, convection, and other minor losses are neglected in the numerical study. Nevertheless, variation is within ±10%, and thus numerical results are validated.

3. Result and discussion

A preliminary numerical study is carried out on the perforated absorber duct insert SAH. The study reveals that a hole diameter of 5 mm perforation hole size is better compared to the 8 mm and 11 mm diameter configuration.[21] This may be due to the fact that smaller diameter holes create a jet-like effect between the upper and lower chamber of the absorber section. This effect reduces as the diameter increases. As the number of holes increases, the pressure difference required to create the crossflow effect also reduces. Hence, the study by Arun *et al.*[21] shows that two-row configurations give higher thermal efficiency than the single-row and three-row configurations. With this background, the hole diameter is kept constant at 5 mm, and the number of rows is two in the absorber duct insert for analysis of various-shaped holes. The hydraulic diameter of the rectangular and triangular hole configurations is kept the same as that of the circular hole configuration.

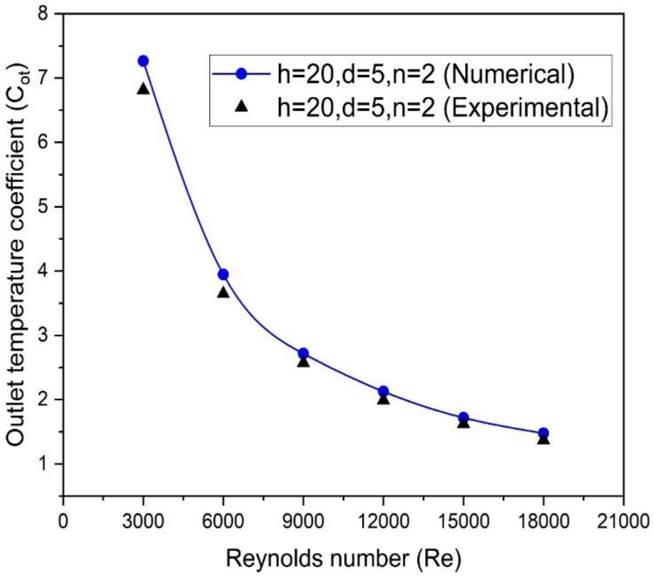

Fig. 5 Validation of the numerical result with the experiment.

Thermal and thermohydraulic efficiencies are calculated using the corresponding inlet temperature, outlet temperature, and pressure drop values for each mass flow rate. Thermal efficiency can be defined as the ratio of the rate of heat gain by the air to the solar radiation heat input. Fig. 6a shows the thermal efficiency versus the Reynolds number plot for circular, triangular, and rectangular-shaped perforation hole configurations.

For all the configurations considered, thermal efficiency increases with the increase in the Reynolds number. The highest thermal efficiencies of 87.33%, 88.23%, and 83.08% are obtained for the circular, rectangular, and triangular hole configurations respectively, at the highest Re of 18000. The higher thermal efficiency for rectangular configuration can be attributed to the greater turbulence that is generated due to the

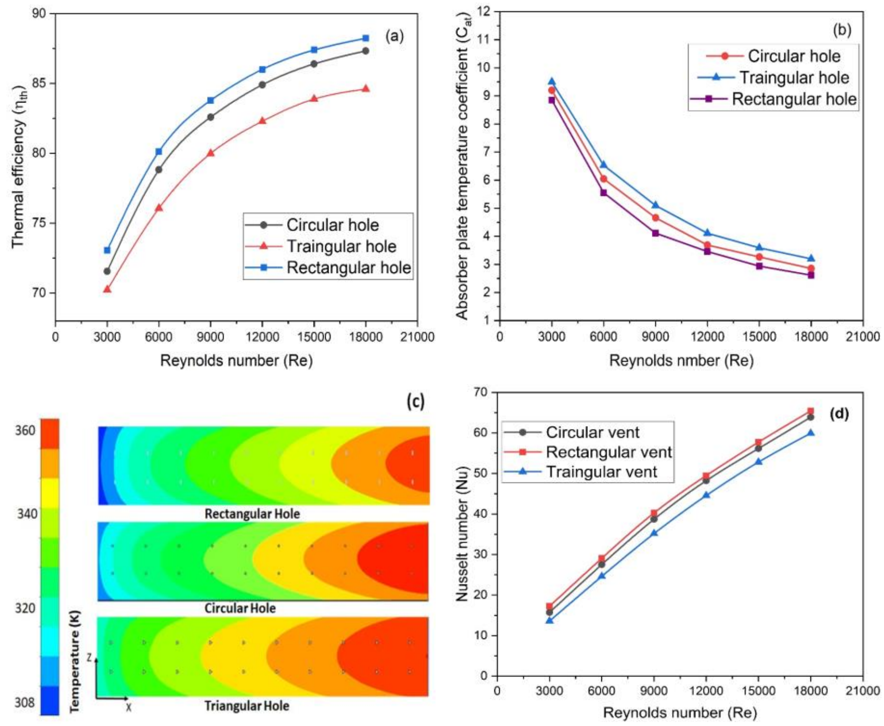

Fig. 6 Thermal performance comparison of the various shaped hole configuration: (a) Thermal efficiency versus Reynolds number; (b) Absorber plate temperature coefficient versus Reynolds number; (c) Contour plot of absorber plate temperature; (d) Nusselt number versus Reynolds number.

four sharp corners of the rectangular holes. In the case of a triangular hole configuration, three sharp corners will cause lower disturbance in the flow stream leading to lower thermal efficiency.

For comparing various configurations, a non-dimensional absorber plate temperature coefficient is defined as given in Eq. (7). The lower temperature of the absorber plate indicates better heat transfer to the flowing air. Fig. 6b shows the variation of the absorber plate temperature coefficient versus the Reynolds number for various configurations considered. It shows a larger drop in absorber surface temperature for rectangular hole configurations compared to that of circular and triangular hole configurations. Fig. 6c shows the contour plot of temperature for the various configuration simulated. The triangular hole configuration shows the highest temperature compared to the other configuration; which is corroborated by the thermal efficiency and absorber plate temperature coefficient trend lines.

Figure 6d shows the variation of the Nusselt number with the Reynolds number. Nusselt number increases as the Reynolds number increases for all the configurations due to the higher heat transfer rate at the higher mass flow range. It is evident that due to the higher heat transfer rate, the rectangular-shaped perforation configuration gives the highest Nu compared to the other two configurations.

Air enters the test section from the inlet duct of the cross-section 200 mm × 30 mm. In the test section, air splits into the upper and lower chamber of the absorber duct insert. Here pressure difference created by the difference in the cross-sectional area causes crossflow from the upper to the lower chamber. Fig. 7a clearly depicts the variation of the pressure across the duct for circular hole configuration.

Due to the variable area in the upper and lower chamber high-pressure zone and low-pressure zone created in the upper and lower chamber causes the crossflow effect. Fig. 7b shows the pressure fluctuation for various configurations considered. Higher pressure fluctuation can be seen at the corner of the triangular hole, and lower pressure fluctuation at the circular-shaped hole configuration.

The lower pressure zone at the lower chamber entrance helps to enhance the velocity and crossflow effect. These pressure fluctuations also cause eddy formation and hence increase the heat transfer rate. Variation of the flow structure along the flow direction can be clearly observed in Fig. 8. The streamline plot at the XY plane shows the air movement from the upper chamber to the lower chamber. The contour plot in the XY plane shows the formation of a fully developed flow at the beginning. Gradually due to the cross-flow effect, flow disturbance at the upper chamber can be visualized for the contour plot. ZX plane top view shows the high-velocity zone at the hole's exit and the eddies' formation near the hole that enhances the turbulence and heat transfer rate.

Figure 9a shows the variation of the pressure with the Reynolds number for the various configuration considered. As the Reynolds number increases, pressure drop increases in all the cases due to higher power requirement to flow. Pressure drop is higher for the perforated absorber duct insert as compared to the plain duct. Among the perforated configurations, the circular hole configuration duct experiences a lesser pressure drop compared to the other two

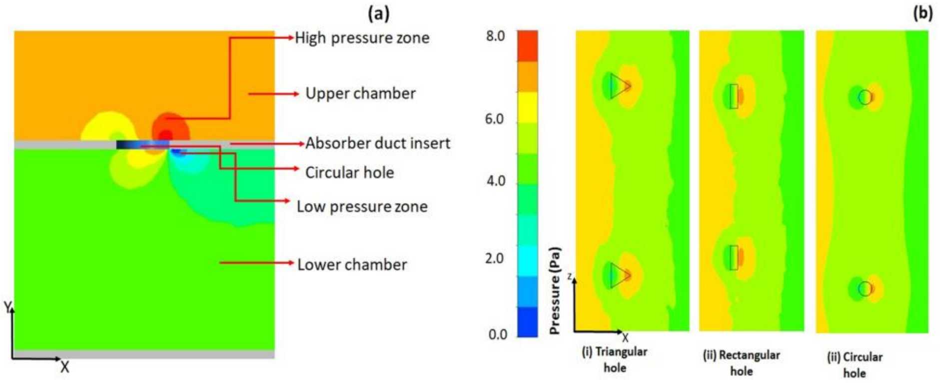

Fig. 7 Variation of the pressure across the duct: (a) Enlarged side view of the circular hole configuration seen across the hole; (b) Side view for all the configurations tested.

configurations considered. Fig. 9b shows the thermo-hydraulic efficiency versus Re plot for the configurations studied. For the lower Reynolds number, thermohydraulic efficiency increases at a higher rate, and this trend continues till the Reynolds number of 15000. At the Reynolds number of 15000, the highest performance is observed. Beyond that efficiency decreases for all the configurations due to higher power requirements than the net gain in the thermal energy. Circular hole configuration shows the highest thermohydraulic efficiency of 83.01% at the Reynolds number of 15000. Rectangular hole and triangular hole configurations also show the highest thermohydraulic performance at the Reynolds number of 15000 with the values being 81.05% and 77.5%, respectively. Due to higher pressure drop, even though the rectangular hole duct configuration shows better performance in terms of thermal efficiency, thermohydraulic efficiency is lesser than the circular hole configuration. The maximum performance obtained in terms of thermal and thermohydraulic efficiency of the present study is compared with a similar study conducted on a double pass flow and perforated absorber plate and shown in Table 2.

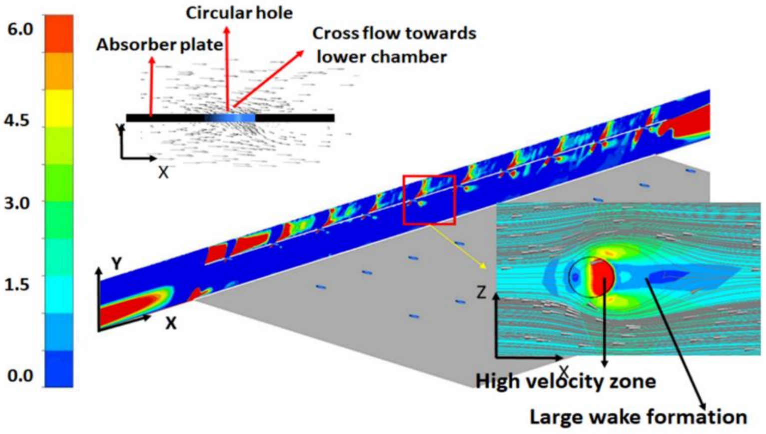

Fig. 8 Variation of the velocity along the flow direction of the duct.

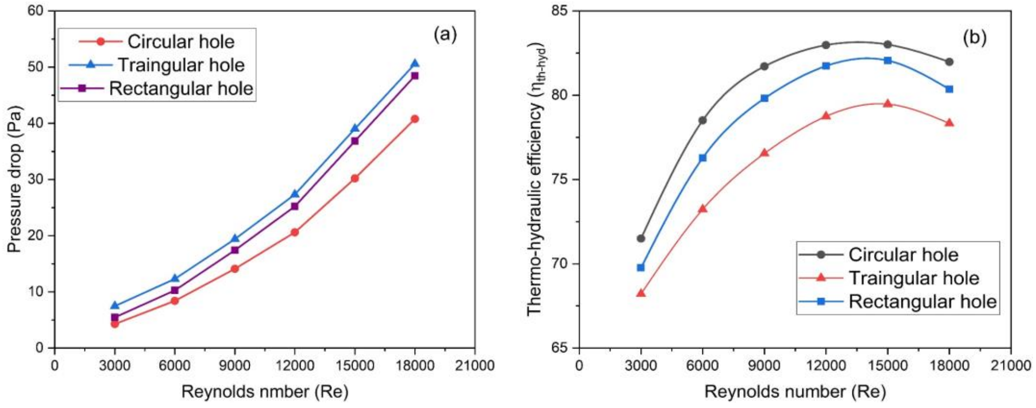

Fig. 9 Thermo-hydraulic performance of the various configuration tested: (a) Pressure drop versus Reynolds number; (b) Thermo-hydraulic efficiency versus Reynolds number.

Table 2. Comparison of thermal and thermohydraulic efficiency of present work with literature.

Author	Concept	Thermal Efficiency	Thermo-hydraulic efficiency
Wang *et al.*[22]	Perforated Back Plate	75%	50%
Ramani *et al.*[23]	Double-pass solar air collector	75%	68%
Mittal *et al.*[24]	Wire mesh-packed solar air heater	81%	75%
Sivakandhan *et al.*[25]	Parallel pass Airflow paths with rectangular and triangular cross-sections at the upper and lower sides	83%	80.12%
Matheswaran *et al.*[26]	Parallel pass jet plate solar air heater	83%	80.12%
Shetty *et al.*[19]	Crossflow SAH	93%	75.5%
Present study	Perforated SAH	88%	83%

4. Conclusion

A numerical study on the perforated absorber duct inserted inside a Solar air heater test section is carried out. A hole diameter of 5 mm and duct height of 20 mm are taken as a reference for the analysis. Hole dimensions for the different shape configurations are selected in such a way that hydraulic diameters remain the same.

All the perforated duct insert configurations show better performance compared to the configuration without perforations. Rectangular hole configuration shows the highest thermal efficiency of 88.23%, followed by circular and triangular configurations due to the generation of greater turbulence near the sharp corners of the rectangular hole. Because of the smooth edge corner, the circular hole configuration causes a lesser pressure drop compared to the rectangular and triangular configurations. Therefore, the highest thermohydraulic efficiency of 83.01% is observed for circular hole configuration compared to rectangular and triangular configurations. This study provides a better design prescription for developing a more efficient solar air heater used in domestic and commercial applications.

Acknowledgments

The experimental and computational facility for conducting this research work was provided by the Department of Mechanical and Manufacturing Engineering, Manipal Institute of Technology, Manipal Academy of Higher Education (MAHE), Manipal. The authors wish to express their gratitude and acknowledge the support provided by the institute in carrying out this research work.

Conflict of interest

There are no conflicts to declare.

Supporting information

Not Applicable.

References

[1] Y. Gao, Z. Wang, D. Ding, W. Li, Y. Ma, Y. Hao, H. Zhang, Novel methods to harness solar radiation for advanced energy applications, *ES Energy & Environment*, 2019, **5**, 1-7, doi: 10.30919/esee8c328.

[2] H. Alshehri, Q. Ni, S. Taylor, R. McBurney, H. Wang, L. Wang, High-temperature solar thermal energy conversion enhanced by spectrally-selective metafilm absorber under concentrated solar irradiation, *ES Energy & Environment*, 2020, **10**, 34-44, doi: 10.30919/esee8c910.

[3] H. S. Arunkumar, K. Vasudeva Karanth, S. Kumar, Review on the design modifications of a solar air heater for improvement in the thermal performance, *Sustainable Energy Technologies and Assessments*, 2020, **39**, 100685, doi: 10.1016/j.seta.2020.100685.

[4] K. Nidhul, A. K. Yadav, S. Anish, S. Kumar, Critical review of ribbed solar air heater and performance evaluation of various V-rib configuration, *Renewable and Sustainable Energy Reviews*, 2021, **142**, 110871, doi: 10.1016/j.rser.2021.110871.

[5] S. Abo-Elfadl, M. S. Yousef and H. Hassan, Assessment of double-pass pin finned solar air heater at different air mass ratios via energy, exergy, economic, and environmental (4E) approaches, *Environmental Science and Pollution Research*, 2020, 1-14, doi: 10.1007/s11356-020-11628-9.

[6] H. M. Yeh, C. D. Ho, J. Z. Hou, The improvement of collector efficiency in solar air heaters by simultaneously air flow over and under the absorbing plate, *Energy*, 1999, **24**, 857-871, doi: 10.1016/s0360-5442(99)00043-2.

[7] S. Satcunanathan, S. Deonarine, A two-pass solar air heater, *Solar Energy*, 1973, **15**, 41-49, doi: 10.1016/0038-092x(73)90004-2.

[8] C. Choudhury, H. P. Garg, Evaluation of a jet plate solar air heater, *Solar Energy*, 1991, **46**, 199-209, doi: 10.1016/0038-092x(91)90064-4.

[9] F. K. Forson, M. A. A. Nazha, H. Rajakaruna, Experimental and simulation studies on a single pass, double duct solar air heater, *Energy Conversion and Management*, 2003, **44**, 1209-1227, doi: 10.1016/s0196-8904(02)00139-5.

[10] R. Chauhan and N. S. Thakur, Heat transfer and friction factor correlations for impinging jet solar air heater, *Experimental Thermal and Fluid Science*, 2013, **44**, 760-767, doi: 10.1016/j.expthermflusci.2012.09.019.

[11] A. M. Aboghrara, B. T. H. T. Baharudin, M. A. Alghoul, N. M. Adam, A. A. Hairuddin, H. A. Hasan, Performance analysis of solar air heater with jet impingement on corrugated absorber plate, *Case Studies in Thermal Engineering*, 2017, **10**, 111-120, doi: 10.1016/j.csite.2017.04.002.

[12] S. Yadav, R. P. Saini, Numerical investigation on the

performance of a solar air heater using jet impingement with absorber plate, *Solar Energy*, 2020, **208**, 236-248, doi: 10.1016/j.solener.2020.07.088.

[13] Y. Wang, M. Boulic, R. Phipps, M. Plagmann, C. Cunningham, Experimental performance of a solar air collector with a perforated back plate in new zealand, *Energies*, 2020, **13**, 1415, doi: 10.3390/en13061415.

[14] M. M. Matheswaran, T. V. Arjunan, D. Somasundaram, Energetic, exergetic and enviro-economic analysis of parallel pass jet plate solar air heater with artificial roughness, *Journal of Thermal Analysis and Calorimetry*, 2019, **136**, 5-19, doi: 10.1007/s10973-018-7727-4.

[15] S. Singh, S. K. Chaurasiya, B. S. Negi, S. Chander, M. Nemś, S. Negi, Utilizing circular jet impingement to enhance thermal performance of solar air heater, *Renewable Energy*, 2020, **154**, 1327-1345, doi: 10.1016/j.renene.2020.03.095.

[16] S. Singh, Experimental and numerical investigations of a single and double pass porous serpentine wavy wiremesh packed bed solar air heater, *Renewable Energy*, 2020, **145**, 1361-1387, doi: 10.1016/j.renene.2019.06.137.

[17] J. P. Jenkins, J. E. Hill, Testing of water-heating collectors according to ASHRAE Standard 93-77, *Sun: Mankind's Future Source of Energy*, 1978, 1021-1028.

[18] W. Gao, W. Lin, T. Liu, C. Xia, Analytical and experimental studies on the thermal performance of cross-corrugated and flat-plate solar air heaters, *Applied Energy*, 2007, **84**, 425-441, doi: 10.1016/j.apenergy.2006.02.005.

[19] S. P. Shetty, N. Madhwesh, K. Vasudeva Karanth, Numerical analysis of a solar air heater with circular perforated absorber plate, *Solar Energy*, 2021, **215**, 416-433, doi: 10.1016/j.solener.2020.12.053.

[20] A. Cortés, R. Piacentini, Improvement of the efficiency of a bare solar collector by means of turbulence promoters, *Applied Energy*, 1990, **36**, 253-261, doi: 10.1016/0306-2619(90)90001-t.

[21] H. S. Arunkumar, S. Kumar, K. Vasudeva Karanth, Experimental study on thermo-hydraulic performance of a solar air heater with rectangular perforated duct inserts, Solar Energy, 2021, **227**, 179-189, doi: 10.1016/j.solener.2021.09.005.

[22] Y. Wang, M. Boulic, R. Phipps, M. Plagmann, C. Cunningham, Experimental performance of a solar air collector with a perforated back plate in new zealand, *Energies*, 2020, **13**, 1415, doi: 10.3390/en13061415.

[23] B. M. Ramani, A. Gupta, R. Kumar, Performance of a double pass solar air collector, *Solar Energy*, 2010, **84**, 1929-1937, doi: 10.1016/j.solener.2010.07.007.

[24] M. K. Mittal, L. Varshney, Optimal thermohydraulic performance of a wire mesh packed solar air heater, *Solar Energy*, 2006, **80**, 1112-1120, doi: 10.1016/j.solener.2005.10.004.

[25] C. Sivakandhan, T. V. Arjunan, M. M. Matheswaran, Thermohydraulic performance enhancement of a new hybrid duct solar air heater with inclined rib roughness, *Renewable Energy*, 2020, **147**, 2345-2357, doi: 10.1016/j.renene.2019.10.007.

[26] M. M. Matheswaran, T. V. Arjunan, D. Somasundaram, Energetic, exergetic and enviro-economic analysis of parallel pass jet plate solar air heater with artificial roughness, *Journal of Thermal Analysis and Calorimetry*, 2019, **136**, 5-19, doi: 10.1007/s10973-018-7727-4.

Author Information

Arunkumar H. S. *presently is working as an Asst. Professor (Senior scale) in the Department of Mechanical and Manufacturing Engineering, Manipal Institute of Technology, Manipal Academy of Higher Education, Manipal, India. He has expertise in the domains of Solar Energy and Thermal power engineering.*

Shiva Kumar *is an Associate Professor (Senior Scale) in the Department of Mechanical and Manufacturing Engineering, at Manipal Institute of Technology, Manipal Academy of Higher Education, Manipal, India. His research interests include refrigeration and air conditioning, Solar air heaters, desiccant based dehumidification and humidification, Engine combustion, Alternative fuels, pollution.*

K. Vasudeva Karanth *is a Professor in the Department of Mechanical and Manufacturing Engineering, at Manipal Institute of Technology, Manipal Academy of Higher Education, Manipal, India. His research interests include turbomachines, Solar air heaters, Photo voltaic cooling amongst others.*